Article:
Tyler, E. orcid.org/0000-0002-3228-5499, Green, A.M. orcid.org/0000-0002-7135-1671 and Goodwin, S.P. orcid.org/0000-0001-6396-581X (2023) Modelling uncertainties in wide binary constraints on primordial black holes. Monthly Notices of the Royal Astronomical Society, 524 (2). pp. 3052-3059. ISSN 0035-8711

https://doi.org/10.1093/mnras/stad2028

Monthly Notices of the ROYAL ASTRONOMICAL SOCIETY

MNRAS **524,** 3052–3059 (2023) https://doi.org/10.1093/mnras/stad2028
Advance Access publication 2023 July 10

Modelling uncertainties in wide binary constraints on primordial black holes

Emily Tyler [1], Anne M. Green [1★] and Simon P. Goodwin [2]

[1] *School of Physics and Astronomy, University of Nottingham, Nottingham, NG7 2RD, UK*
[2] *Department of Physics and Astronomy, University of Sheffield, Sheffield, S3 7RH, UK*

Accepted 2023 July 4. Received 2023 June 14; in original form 2022 July 20

ABSTRACT

Dark matter in the form of compact objects with mass $M_{\rm co} \gtrsim 10\,{\rm M}_\odot$ can be constrained by its dynamical effects on wide binary stars. Motivated by the recent interest in primordial black hole dark matter, we revisit the theoretical modelling involved in these constraints. We improve on previous studies in several ways. Specifically, we (i) implement a physically motivated model for the initial wide-binary semimajor axis distribution, (ii) include unbound binaries, and (iii) take into account the uncertainty in the relationship between semimajor axis and observed angular separation. These effects all tend to increase the predicted number of wide binaries (for a given compact object population). Therefore, the constraints on the halo fraction in compact objects, $f_{\rm co}$, are significantly weakened. For the wide binary sample used in the most recent calculation of the constraints, we find the fraction of halo dark matter in compact objects is $f_{\rm co} < 1$ for $M_{\rm co} \approx 300\,{\rm M}_\odot$, tightening with increasing $M_{\rm co}$ to $f_{\rm co} < 0.26$ for $M_{\rm co} \gtrsim 1000\,{\rm M}_\odot$.

Key words: binaries: general – Galaxy: halo – dark matter.

1 INTRODUCTION

There is strong evidence from cosmological and astronomical observations that ≈ 85 per cent of the matter in the Universe is in the form of cold, non-baryonic dark matter (DM), see e.g. Bertone, Hooper & Silk (2005) for a review. Traditionally the most popular DM candidates have been new elementary particles, such as weakly interacting massive particles or axions. However, the discovery of gravitational waves from mergers of tens of solar mass black holes by LIGO-Virgo (Abbott et al. 2016) has led to a surge of interest in primordial black holes (PBHs) as a DM candidate (Bird et al. 2016; Carr, Kuhnel & Sandstad 2016; Sasaki et al. 2016). PBHs are black holes that may form in the early Universe, for instance from the collapse of large density perturbations (Zel'dovich & Novikov 1967; Hawking 1971).

There are various constraints on the abundance of PBHs with mass $M_{\rm PBH} \gtrsim 1\,{\rm M}_\odot$ from gravitational microlensing (Diego et al. 2018; Zumalacarregui & Seljak 2018; Blaineau et al. 2022; Esteban-Gutiérrez et al. 2022), gravitational waves from mergers of binaries (Sasaki et al. 2016; Ali-Haïmoud, Kovetz & Kamionkowski 2017), their dynamical effects on stars in wide binaries (Yoo, Chaname & Gould 2004; Quinn et al. 2009; Monroy-Rodríguez & Allen 2014) and in dwarf galaxies (Brandt 2016), and the radiation emitted due to accretion of gas onto PBHs (Ricotti, Ostriker & Mack 2008; Gaggero et al. 2017). For reviews, with extensive reference lists, see e.g. Carr & Kuhnel (2020) and Green & Kavanagh (2021). The increased interest in PBH DM motivates a careful reanalysis of these constraints. For instance, the constraints from the temperature anisotropies in the cosmic microwave background, due to the effects of PBHs on the recombination history of the Universe, have been found to be significantly weaker than previously thought (Ali-Haïmoud & Kamionkowski 2017; Poulin et al. 2017).

In this paper, we focus on the constraints on multisolar mass compact objects in the halo of the Milky Way (MW) from their dynamical effects on wide binary stars. While this is motivated by the recent interest in PBHs as a DM candidate, these constraints apply to any compact object DM. Close encounters between binary stars and massive compact objects increase the energies and semimajor axes of the binaries, and potentially disrupt some of the binaries. Observations of the semimajor axis distribution of wide binaries in the MW can, therefore, potentially constrain the abundance of compact objects. For perturbers with mass $M_{\rm p} \gtrsim 10^3\,{\rm M}_\odot$ the closest encounter dominates, while for lighter perturbers it is necessary to take into account the cumulative diffusive effects of multiple interactions (Bahcall, Hut & Tremaine 1985; Binney & Tremaine 2008).

Bahcall et al. (1985) used wide binaries in the MW disc to constrain the fraction of the local mass density in compact objects. Yoo et al. (2004) then used a sample of 90 wide halo binaries compiled by Chanamé & Gould (2004) to constrain the fraction of the MW halo in compact objects. They found that compact objects with mass $M_{\rm co} > 43\,{\rm M}_\odot$ could not make up all of the halo, and objects with mass $M_{\rm co} \gtrsim 10^3\,{\rm M}_\odot$ were constrained to make up less than 20 per cent of the halo, at 95 per cent confidence.

Quinn et al. (2009) highlighted that these constraints are very sensitive to the widest binaries. They carried out radial velocity

★ E-mail: anne.green@Nottingham.ac.uk

measurements of four of the widest binaries in the Chanamé & Gould (2004) sample, and found that the second widest binary was in fact not a binary, as the two stars have significantly different radial velocities. Without this spurious binary, the mass above which compact objects were excluded from making up all of the halo increased to $M_{\rm co} \sim 500\,{\rm M}_\odot$. The radial velocities, along with the proper motions, also allow the orbits of the binaries to be calculated. The orbits found by Quinn et al. (2009) extend to radii (20–60) kpc. In this case the average DM density the binaries experience is significantly, (50–90) per cent, smaller than the local (i.e. at the solar radius) DM density, which further weakens the constraint. Quinn et al. (2009) concluded that the Chanamé & Gould (2004) sample was too small to place meaningful constraints on the halo fraction of compact objects.

Monroy-Rodríguez & Allen (2014) calculated constraints using 251 halo wide binaries from a catalogue compiled by Allen & Monroy-Rodríguez (2014). 160 of these binaries had radial velocity measurements, allowing their orbits to be calculated. Using the binaries which spend the smallest fraction of their time in the Galactic disc, they found that compact objects with $M_{\rm co} \gtrsim 5\,{\rm M}_\odot$ are excluded from making up all of the halo, and objects with mass $M_{\rm co} \gtrsim 10^2\,{\rm M}_\odot$ make up less than 10 per cent, at 95 per cent confidence. Contrary to Quinn et al. (2009), they found that the average DM densities experienced by the wide binaries are not significantly different from the local density.

In this paper, we revisit the modelling assumptions in these analyses, refining several aspects. In particular, previous work assumed that the initial binary semimajor axis distribution is log-flat or a power law, while we use an initial distribution motivated by simulations of the formation of wide binaries during the dissolution of large star clusters (Kouwenhoven et al. 2010; Griffiths 2019). We also include unbound binaries in our comparison with observations and take into account the uncertainty in calculating the observed angular separation of a binary from its semimajor axis. We outline our method in Section 2, present and discuss our results in Section 3, and conclude with a summary in Section 4.

2 METHOD

2.1 Binary sample

To illustrate the effects of theoretical modelling on the constraints, we use the catalogue of halo wide binaries compiled from various sources by Allen & Monroy-Rodríguez (2014). This catalogue was used by Monroy-Rodríguez & Allen (2014) to calculate the most recent wide binary constraints on the abundance of compact objects (that are quoted in reviews of PBH DM e.g. Carr & Kuhnel 2020; Green & Kavanagh 2021).

As discussed by Chanamé & Gould (2004), constructing a reliable large catalogue of halo binaries, without selection biases, is non-trivial. Halo binaries need to be distinguished from disc binaries and, as emphasized by Quinn et al. (2009), radial velocity measurements are required to eliminate chance associations. Coronado et al. (2018) constructed a catalogue of halo binaries using sloan digital sky survey data, however this sample only covers projected separations less than ~ 0.1 pc.

GAIA (Gaia Collaboration 2018) offers the possibility of constructing a large, consistent catalogue of halo wide binaries. However at this time there is no definitive sample of halo binaries (see e.g. Oelkers, Stassun & Dhital 2017; Oh et al. 2017; Tian et al. 2020, for work in this direction).

2.2 Simulations

2.2.1 *Interactions between perturbers and wide binaries*

Our simulations of interactions between perturbers[1] and wide binaries largely follow Yoo et al. (2004). We assume that all binaries are composed of stars which each have mass $0.5\,{\rm M}_\odot$ and that the distribution of the relative velocities of the binaries and perturbers, $f(v_{\rm rel})$, is Maxwellian with dispersion $\sigma_{\rm rel} = 220\,{\rm km\,s^{-1}}$.

When we compare simulated binary distributions with observations in Section 2.3 below, the initial binary semimajor axis distribution is taken into account using a scattering matrix formalism, as in Yoo et al. (2004). In our initial simulations, for simplicity and following previous work, we use a semimajor distribution which is log-flat between 10 and $10^{5.5}$ au, and assume that the square of the initial eccentricity is uniformly distributed between 0 and 1 (i.e. thermal).

As in previous work (Yoo et al. 2004; Quinn et al. 2009; Monroy-Rodríguez & Allen 2014), we do not include perturbations from giant molecular clouds (GMCs) or the effects of Galactic tides. Due to their low number density in the halo, the impact of GMCs on halo wide binaries is expected to be small, and neglecting it is a conservative assumption. Galactic tides are smaller for halo wide binaries than for the disc binaries studied in Jiang & Tremaine (2010), and likewise including their effects would act to tighten the constraints. We have also assumed that the PBHs are smoothly distributed and are not themselves in binaries. Some PBHs are expected to form binaries in the early Universe (Nakamura et al. 1997; Ali-Haïmoud et al. 2017), and PBH clusters form not long after matter–radiation equality (Afshordi, McDonald & Spergel 2003; Inman & Ali-Haïmoud 2019). The evolution of these clusters, and in particular the disruption of PBH binaries within them, is a challenging problem and the present day spatial distribution of PBHs within galaxies is not yet understood in detail.

Unlike previous work on constraints on compact object DM from halo binaries, we include unbound binaries in our comparison with observed binaries. Yoo et al. (2004) argued that disrupted binaries quickly diffuse to large separations, beyond those probed observationally. However, Jiang & Tremaine (2010) included unbound systems in their study of the effects of perturbers on disc binaries using diffusion equations. They found that the stars from unbound binaries have small relative velocities, which would lead them to be detected as binaries by surveys. Furthermore, they also found that some unbound binaries can become rebound.

The rate at which encounters with impact parameter between b and $b + {\rm d}b$ and relative velocity between $v_{\rm rel} + {\rm d}v_{\rm rel}$ occur, $\dot{C}$, is given by

$$\dot{C} = n_{\rm p} v_{\rm rel} 2\pi b\,{\rm d}b f(v_{\rm rel})\,{\rm d}v_{\rm rel}, \quad (1)$$

where $n_{\rm p} = \rho/M_{\rm p}$ is the perturber number density and ρ and $M_{\rm p}$ are the perturber mass density and mass, respectively. We consider perturber masses in the range $1\,{\rm M}_\odot < M_{\rm p} < 3 \times 10^3\,{\rm M}_\odot$ and fix ρ to the standard value for the local DM density, $0.009\,{\rm M}_\odot\,{\rm pc}^{-3}$ (e.g. de Salas & Widmark 2021), however the constraints can be straight forwardly rescaled to other values of the local DM density.

We have found (see fig. 3.5 of Tyler 2022) that encounters which cause a fractional change in the binary energy less than 0.1 per cent

[1]We are specifically interested in the case of PBH DM, however the constraints apply to any compact object DM, and therefore we use these terms, and 'perturber' interchangably.

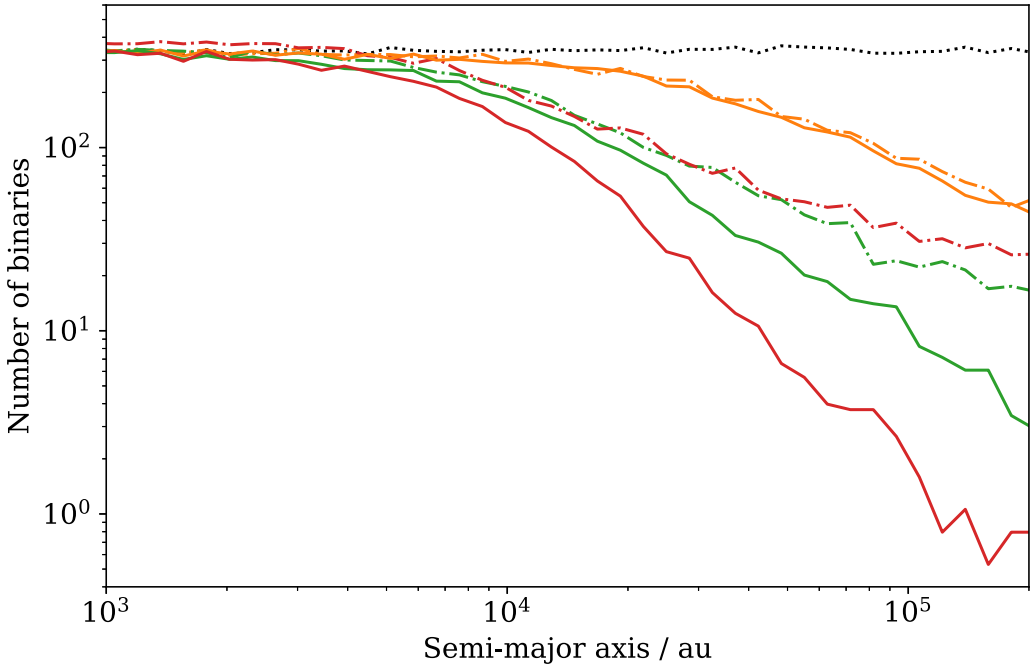

Figure 1. The final semimajor axis distribution of 10^5 binaries composed of stars with mass $0.5\,M_\odot$ evolved for 10 Gyr in a population of perturbers with a Maxwellian relative velocity distribution with dispersion $\sigma_{\rm rel} = 220\,{\rm km\,s^{-1}}$, mass density $\rho = 0.009\,M_\odot\,{\rm pc^{-3}}$ and masses 10 (orange lines), 100 (green), and $1000\,M_\odot$ (red). The dot–dashed lines are for the full binary population (bound and unbound binaries), while the solid lines show only the binaries that remain bound at all times. The initial log-flat binary semimajor axis distribution is shown by the black dotted line.

have a negligible (less than 0.1 per cent) effect on the semimajor axis distribution, therefore we do not include these encounters in our simulations. We calculate the number of interactions expected within a time $T = 10\,{\rm Gyr}$, roughly equally to the age of the MW. For each individual binary the actual number of encounters experienced is drawn from a Poisson distribution and the impact parameter and relative velocity of each encounter are found from the distributions in equation (1).

The relative velocity between the perturber and binary is always much larger than the orbital velocities of the binary stars. Therefore, the stars can be treated as stationary during an encounter and the impulse approximation used to calculate its effect (e.g. Binney & Tremaine 2008). The positions of the stars are unperturbed, while the changes in their velocities are perpendicular to the trajectory of the perturber and given by

$$\Delta v_i = \frac{2GM_{\rm p}}{v_{\rm rel} b_i}\frac{\mathbf{b}_i}{b_i}, \tag{2}$$

where $\mathbf{b}_i$ is the impact parameter to star i.

Binaries are evolved in time between encounters. For bound binaries the time between encounters is much longer than the period of the binary, so we do this by taking a random value for the mean anomaly between 0 and 2π and converting this (via Kepler's equation) to a future true anomaly. The hyperbolic orbits of unbound binaries are not periodic, so in this case we evolve the binary's eccentric anomaly forwards in time exactly. The position and velocity vectors of the two stars before each encounter are calculated from their semimajor axis, eccentricity and orbital phase (true anomaly).

Fig. 1 shows the final semimajor axis distribution for simulations with a log-flat initial binary semimajor axis distribution and perturbers with density $\rho = 0.009\,M_\odot\,{\rm pc^{-3}}$ and masses $M_{\rm p} = 10$, 10^2, and $10^3\,M_\odot$. It shows both the full binary population (dot–dashed lines) and also just the binaries which remain bound throughout the whole simulation (solid lines), i.e. the result that would be obtained by discarding unbound binaries. We see that for $M_{\rm p} = 10^2$ and $10^3\,M_\odot$ (green and red lines, respectively) the two distribution differ significantly for $a \gtrsim 10^4$ au, and hence discarding unbound binaries significantly underestimates the abundance of the widest observed apparent binaries. As mentioned previously, Jiang & Tremaine (2010) find that disrupted binaries in the Galactic disc have very small relative velocities. For perturbers larger than $\sim 1\,M_\odot$, however, the increase in relative velocity due to encounters is more significant (equation A2 Yoo et al. 2004). We note that our results for binaries that remain bound throughout are in good agreement with previous work by Yoo et al. (2004) and Monroy-Rodríguez & Allen (2014).

The large abundance of unbound wide binaries for $M_{\rm p} = 10^3\,M_\odot$ is likely due to the low number density of perturbers, which decreases with increasing perturber mass (for constant perturber mass density). Even though encounters with $M_{\rm p} = 10^3\,M_\odot$ are more likely to break the binaries, multiple encounters are required to give the binaries sufficient relative velocity to drift apart within the time-scale of the simulation. This may also explain why for $M_{\rm p} = 10\,M_\odot$ there are very few unbound binaries; these binaries have experienced a large number of encounters giving them sufficient relative velocity to drift far apart by the end of the simulation.

2.2.2 *Orbits of binaries*

It is useful to calculate the orbits of the wide binaries within the MW potential for two reasons. First, each binary experiences an orbit-dependent time-varying DM density. This can be taken into account by finding the time-averaged DM density along each binary orbit, and scaling the constraint on the perturber density by the mean time-averaged DM density divided by the value of the local DM density (Quinn et al. 2009). Secondly, binaries will experience perturbations from stars when passing through the Galactic disc, and hence binaries

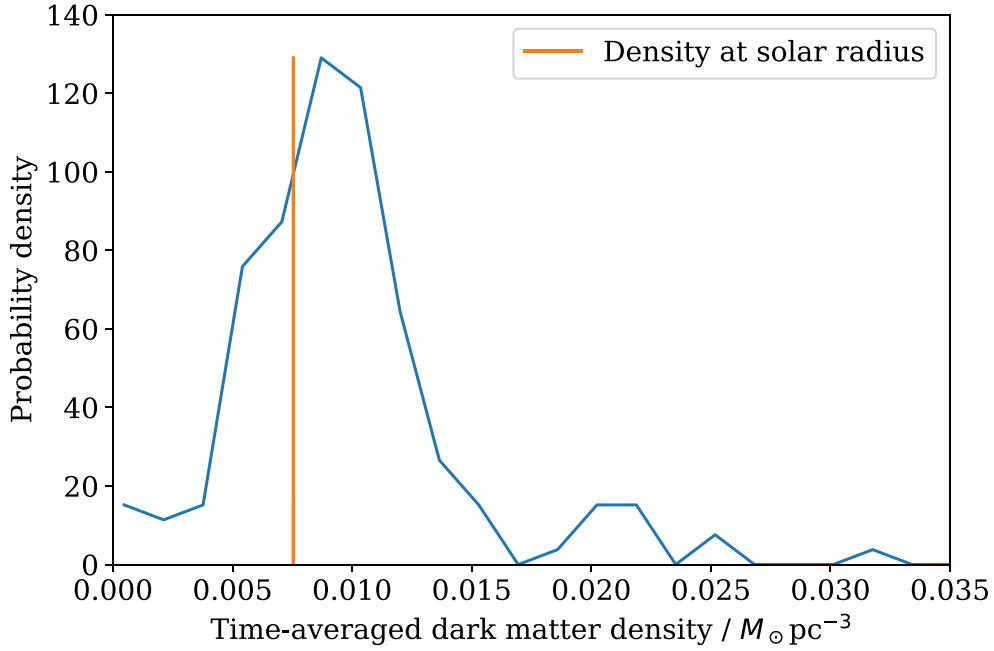

Figure 2. The probability distribution of the time-averaged DM density calculated along the orbits of 160 binaries from Allen & Monroy-Rodríguez (2014) that it is possible to calculate orbits. The orange vertical line shows the DM density at the solar radius, 0.00754 $M_\odot$ pc^{-3}.

that spend the smallest fraction of their orbits within the Galactic disc are more powerful for constraining perturbers in the halo. Monroy-Rodríguez & Allen (2014) classified the binaries as 'most halo-like' according to the fraction of time their orbit spends within the disc ($|z| < 500$ pc).

We calculated the binary orbits for the 160 binaries in the Allen & Monroy-Rodríguez (2014) catalogue [2] which has sufficient data to do this using the GALPY PYTHON package (Bovy 2015). For each binary we use the most recent data from the SIMBAD data base (Wenger et al. 2000), usually from GAIA DR2 (Gaia Collaboration 2018). We used the `MWPotential2014` model in GALPY, which has a Navarro–Frenk–White density profile (Navarro, Frenk & White 1997) for the MW halo, along with potentials for the disc and bulge. While this model is not intended to be the best current model of the MW, its parameters are similar to those obtained from, e.g. fits to rotation curve data (Eilers et al. 2019), and it is sufficiently accurate for our purpose. We find the mean time-averaged DM density for the 160 binaries is ~ 40 per cent larger than the DM density at the solar radius. Quinn et al. (2009) found substantially smaller time-averaged DM densities for the widest binaries that they studied. However, like Monroy-Rodríguez & Allen (2014), we find that the orbit for NLTT10536 reaches a maximum z value of around 5 kpc, whereas the orbit calculated by Quinn et al. (2009) extended to $z \approx 40$ kpc. Also, using the most recent determination of its distance, proper motion, and radial velocity, we find an orbit for NLTT16394 which is confined to smaller values of z and R than previously found (Quinn et al. 2009; Monroy-Rodríguez & Allen 2014)

The probability density of the time-averaged DM densities for the 160 binaries it is possible to calculate orbits for is shown in Fig. 2. The distribution of time-averaged DM densities experienced by the binaries is not too wide (full width at half maximum 0.007 $M_\odot$ pc^{-3}). This suggests that simply scaling the constraint on the perturber density by the mean time-averaged DM density should capture the effect of the varying DM density experienced by the binaries.

[2]Online data from https://cdsarc.cds.unistra.fr/viz-bin/cat/J/ApJ/790/158.

2.3 Comparison with observations

2.3.1 Initial semimajor axis distribution

A model is required for the initial semimajor axis separation distribution from which the current distribution has evolved. Unfortunately, it is extremely unclear what that initial distribution should be. Previous work on wide binary disruption (Weinberg, Shapiro & Wasserman 1987; Yoo et al. 2004; Quinn et al. 2009; Jiang & Tremaine 2010; Monroy-Rodríguez & Allen 2014) used a power law distribution, $\propto a^{-\alpha}$, which is the simplest generalization of Öpik's Law, a log-flat distribution. It is not at all obvious that this simple distribution is a good model for the initial wide binary semimajor axis distribution (see also Tian et al. 2020).

Binary semimajor axis distributions usually seem to follow a roughly log-normal distribution with a peak at tens to hundreds of au depending on the primary mass (see e.g. Raghavan et al. 2010; Duchêne & Kraus 2013; Ward-Duong et al. 2015). The best understood sample of binary separations are local field G dwarfs (Raghavan et al. 2010) which have a log-normal separation distribution which peaks at ~30 au, with a variance of 1.5 in the log (so roughly two thirds of systems lie between 1 and 1000 au).

Local field G dwarfs have a few per cent of very wide binaries beyond 10^4 au, which is usually modelled as the exponential tail of the G dwarf log-normal. However, it is not clear that this is a good way of modelling the wide binary tail. The formation mechanism(s) of very wide binaries, with semimajor axis $>10^4$ au, are not understood. The peaks of binary distributions (at tens to hundreds of au) are thought to arise from core and/or disc fragmentation during star formation (see Goodwin et al. 2007; Duchêne & Kraus 2013; Reipurth et al. 2014). However, systems with separations $>10^4$ au are much wider than the size of star forming cores and so it is uncertain how they

arise. The most likely mechanism suggested so far is 'soft capture' (Kouwenhoven et al. 2010; Moeckel & Bate 2010; Moeckel & Clarke 2011), where a wide binary is formed by the chance proximity of two stars with low relative velocities during the dissolution of a star cluster or star forming region.

Simulations of soft capture show that the rate is low, but that very wide binaries can be formed. Griffiths (2019) carried out simulations of the dissolution of clusters with different levels of (fractal) substructure in the initial star cluster (c.f. Kouwenhoven et al. 2010). From their simulations we find that a power-law distribution is a good fit to the wide binaries formed via soft capture (see e.g. their fig. 5.7), with the slope decreasing from $\alpha = 0.9$ to 0.7 as the level of substructure decreases. This could well appear like an exponential tail in the broader distribution of separations (as current data is too poor to show any features of different formation mechanisms).

How many wide binaries we would expect is another unknown. The fraction of wide binaries in the local field G dwarf population is a few per cent (depending on exactly where one draws the line for wide binaries, see e.g. Tokovinin & Lépine 2012). However, the local field population should have been processed to some degree by other field stars in exactly the same way a PBH population would process the halo binaries. Therefore, this provides a lower limit on wide binary production in what are now Galactic disc field stars. If we assume soft capture as the mechanism then we would not expect a metallicity-dependence on the primordial wide binary fraction.[3]

Therefore, as well as considering a pure power law for the initial binary semimajor axis distribution (motivated by our fits to simulations of soft capture), we also study an initial distribution where in addition primordial binaries make up a variable fraction, $1 - A$, of the total population between $a_{\rm min} = 30$ and 2×10^4 au. We assume that the primordial binaries have a log-normal distribution with mean $\mu = 100$ au and log width $\sigma = 1.5$ (which is closer to the local pre-main sequence binary population than the local field, see Duchêne & Kraus 2013).

2.3.2 Binary separations

The observed separation of a system is the angular separation, which depends on its semimajor axis, eccentricity, phase, inclination, orientation, and distance. From a single observation of a separation on the sky it is impossible to determine the true semimajor axis in anything other than a purely statistical way. Yoo et al. (2004) calculated a theoretical angular separation distribution by convolving the projected separation distribution of their simulated binaries with their assumed (inverse) distance distribution. Monroy-Rodríguez & Allen (2014) instead compared the semimajor axis distribution of simulated and observed binaries, using a statistical relationship between semimajor axis and angular separation to estimate the observed semimajor axes.

The problem with using a statistical relationship between the instantaneous separation and the semimajor axis is that it only holds for a 'typical' binary. On average, the semimajor axis of a binary is slightly larger than the observed separation (how much larger depends on the assumed eccentricity distribution). However, some binaries (high eccentricity systems at apastron, oriented such that we see the 3D separation in 2D) will be observed with a separation of approximately twice the semimajor axis. Such systems are rare, but will tend to fall at the widest extreme of the distribution. Therefore, at the widest end of the distribution this would tend to over-estimate the semimajor axes. For this reason we compare the projected separations of our theoretical distribution with the observed distribution, by randomizing the viewing angles, rather than attempting to turn the observed separation distribution into a semimajor axis distribution.

To calculate the predicted separation distribution for a given initial semimajor axis distribution, we use the same scattering matrix formalism as Yoo et al. (2004). Since each binary evolves independently, then the expected number of binaries with projected separation r_j, $P(r_j, M_{\rm p}, \rho)$, is given by

$$P(r_j, M_{\rm p}, \rho) \propto a_j \, S_{ij}(M_{\rm p}, \rho) \, q(a_j), \tag{3}$$

where $q(a)$, is the probability density of the initial semimajor axis distribution and the scattering matrix, $S_{ij}(M_{\rm p}, \rho)$, is the number of simulated binaries with initial semimajor axis in the i-th logarithmically spaced bin centred at a_i that have final projected separation r_j for a simulation with perturber mass $M_{\rm p}$ and DM density ρ. The factor of a_j appears because our semimajor axis bins are logarithmically spaced.

2.3.3 Statistical analysis

Previous work has used likelihood analysis (Yoo et al. 2004) or the Kolmogorov–Smirnov (K–S) test (Monroy-Rodríguez & Allen 2014) to compare simulated and observed binary distributions. Both of these methods have drawbacks for this analysis. Likelihood analysis doesn't provide information about how good a fit the best fit is, while the K–S test is less sensitive to differences in the extremes of distributions, which is suboptimal as the widest binaries are most affected by perturbers. The classical χ^2 test is not valid if the number of samples in any bin is small, which is the case for the widest binaries. We, therefore, use a modified version of the χ^2 test, which provides p values, is valid for small sample sizes, and is equally sensitive to deviations across the whole range of the distributions.

The modified Y^2 statistic (Lucy 2000), is rescaled so that its variance is fixed to be equal to twice its mean, and hence the standard translation of χ^2 values into p values is valid, even for small samples. The Y^2 statistic is defined as

$$Y^2 = \nu + \sqrt{\frac{2\nu}{2\nu + \Sigma_i n_i^{-1}}} \left(\chi^2 - \nu\right), \tag{4}$$

where n_i is the expected number of binaries in the i-th bin. The number of degrees of freedom, ν, is equal to the number of bins minus the number of fitted parameters plus one as the n_i's have been normalized to match the total observed number of binaries. The χ^2 statistic is given, as usual, by

$$\chi^2 = \sum_i \frac{(N_i - n_i)^2}{n_i}, \tag{5}$$

where N_i is the number of observed binaries in the i-th bin and the sum is over all bins with non-zero N_i.

3 RESULTS AND DISCUSSION

We calculate the Y^2 statistic as a function of perturber mass, $M_{\rm p}$, and density, ρ, the fraction of the binaries that have power-law semimajor axis distribution initially, A, and the slope of the power law, α. For each $M_{\rm p}$ and ρ combination we find the minimum value of Y^2, $Y^2_{\rm min}(M_{\rm p}, \rho)$. We first check that the best fit is a sufficiently good

[3]El-Badry & Rix (2019) find a very slight excess of metal rich field wide, (5000–50 000) au, binary systems over metal poor systems, but the two are very similar.

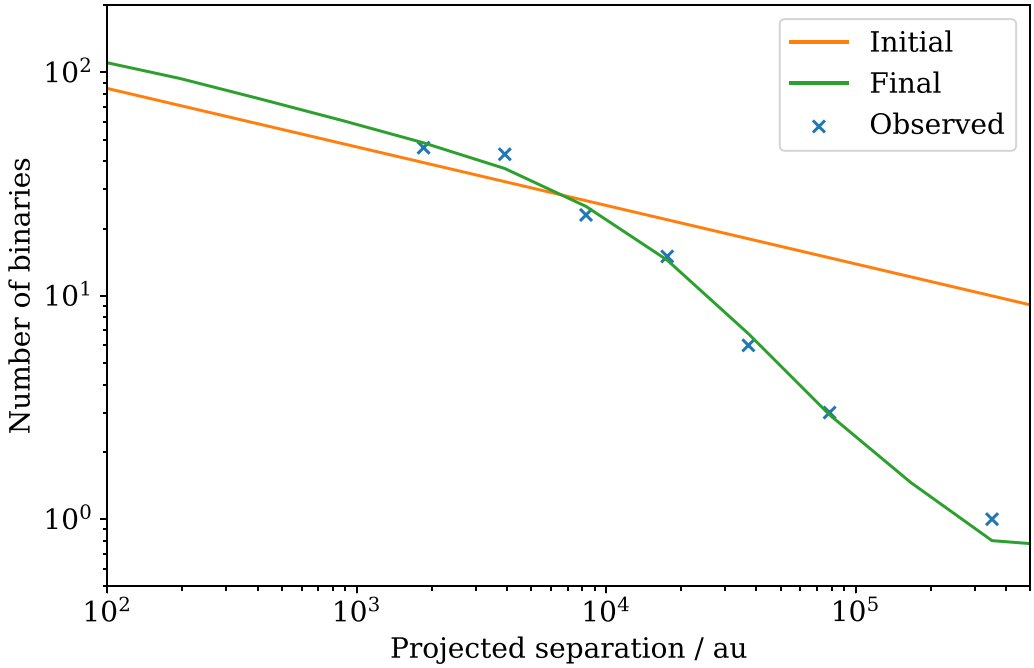

Figure 3. The best-fitting final projected separation distribution (green line) compared with the observed separation distribution (blue crosses). The corresponding initial distribution (orange line), which has parameters $\alpha = 1.26$ and $A = 1.00$ is also shown. The best-fitting perturber mass and density are $M_p = 30\,M_\odot$ and $\rho = 0.012\,M_\odot\ \mathrm{pc}^{-3}$, respectively.

fit by comparing the global minimum value of Y^2 and $Y^2_{\rm min}$, with the number of degrees of freedom, ν. Here we have two fitted parameters (A and α) and seven bins, so $\nu = 7 - (2 + 1) = 4$. The global best fit has $\alpha = 1.26, A = 1, M_p = 30\,\mathrm{M}_\odot$, and $\rho = 0.012 M_\odot\,\mathrm{pc}^{-3}$. It has $Y^2_{\rm min} < 3$ and hence is indeed a good fit to the data. Fig. 3 compares the best fit projected separation distribution with the observed separation distribution, and also shows the corresponding initial separation distribution.

Next, we calculate constraints on M_p and ρ by finding the pairs of values for which

$$\Delta Y^2(M_p, \rho) = Y^2_{\rm min}(M_p, \rho) - Y^2_{\rm min} = \mathrm{inverse}\,(1 - \mathrm{cdf}(p))\,, \qquad (6)$$

where $p = 0.05$ for 2σ constraints, and cdf is the cumulative distribution function of the χ^2 distribution with 2 degrees of freedom, since we are now finding constraints on two parameters (M_p and ρ). We do this for both $A = 1$, i.e. a pure power law distribution for the initial binary distribution, and $0 < A < 1$, i.e. allowing a varying fraction of the distribution to be log-normal. Finally, as discussed in Section 2.2.2, we rescale our constraints by a factor of 0.71 to take into account the average DM density experienced by the binaries along their orbits.

Our constraints on the perturber mass, M_p, and density, ρ, are shown in Fig. 4. We compare our (very similar) 2σ constraints for $A = 1$ (orange line) and $0 < A < 1$ (blue line) with the Monroy-Rodríguez & Allen (2014) constraints from their 100 and 25 'most halo like' binary samples (green solid and dashed lines, respectively). For values of M_p larger than those plotted, the Monroy-Rodríguez & Allen (2014) constraints are expected to be roughly constant.

We tested the validity of comparing 25 observed binaries with our simulations and found that randomly choosing groups of 25 binaries resulted in constraints that varied significantly. This is due to the large stochasticity in the distribution of observed angular separations from a semimajor axis distribution when the number of binaries is small. This suggests that a much larger sample of halo wide binaries is required to provide any meaningful constraints. Therefore, we only present our constraints calculated using the full sample of binaries to avoid this stochasticity. Fig. 7 of Monroy-Rodríguez & Allen (2014) indicates that they were able to calculate reliable constraints from small sub-populations of binaries. This difference is likely to be because they compare 'virtual' binaries, constructed from 500–10 000 simulated binaries, with the semimajor axis of observed binaries calculated by assuming there is a one-to-one relationship between projected separation and semimajor axis. This assumption is an oversimplification that does not take into account the varied phases and orientations of the observed binaries.

Our constraint is significantly weaker than that from Monroy-Rodríguez & Allen (2014). We find $f_{\rm co} < 1$ for $M_p \approx 300\,\mathrm{M}_\odot$, tightening with increasing M_p to $f_{\rm co} < 0.26$ for $M_p \gtrsim 1000\,\mathrm{M}_\odot$. An obvious question is "why are our constraints so much weaker than those of Monroy-Rodríguez & Allen (2014)?". To restate the obvious – compact objects destroy wide binaries, and the wider the binary, the more susceptible to destruction it is. Therefore, the constraints on the allowed compact object density are extremely sensitive to the number of very wide binaries, and the exact values of the semimajor axes. We include two effects that Monroy-Rodríguez & Allen (2014) did not, both of which act to increase the number of very wide binaries predicted for any particular initial semimajor axis distribution and perturber population. Consequently, the abundance of perturbers required to reduce the abundance of the widest binaries below that which we observe is larger.

First, we do not discard unbound binaries. This means there are systems with wide separations which, from a single observation, would be indistinguishable from a (very weakly) bound 'true' binary. This increases the number of very wide systems that could potentially be observed.

Secondly, by projecting our theoretical distribution into observed separations we correctly allow for systems to be observed where the separation is significantly larger than the semimajor axis (up to a

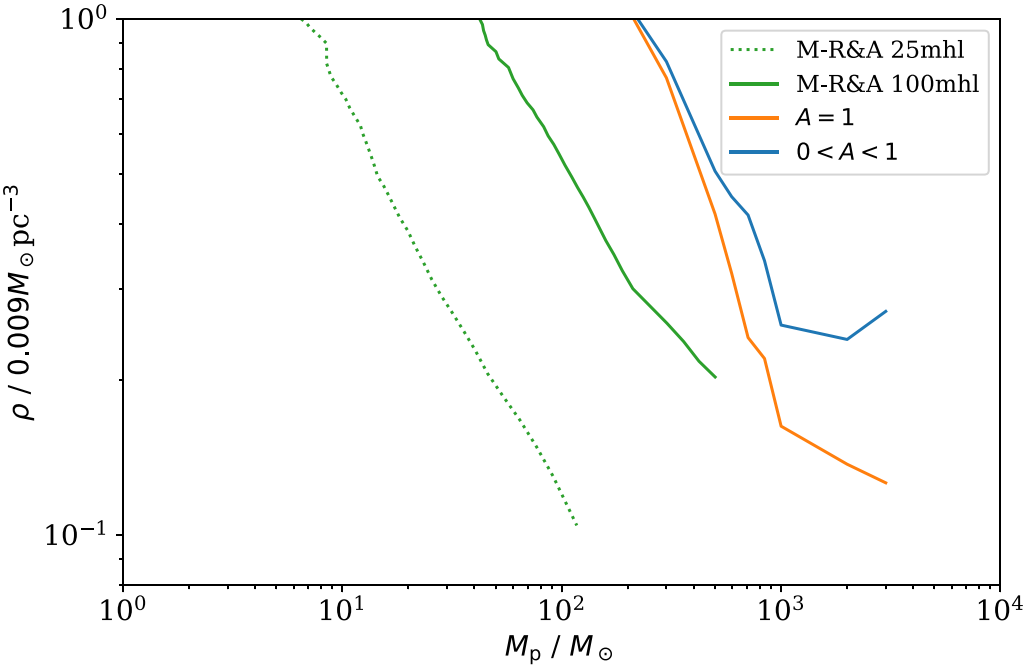

Figure 4. Two sigma constraints on the perturber density, ρ, as a function of the perturber mass, M_p. The orange and blue lines show our constraints for $A = 1$ (initial binary semimajor axis distribution is a pure power law) and $0 < A < 1$ (allowing a varying fraction of the initial distribution to be log-normal), respectively. The dotted and solid green lines are the Monroy-Rodríguez & Allen (2014) constraints for their 25 and 100 most halo like binaries, respectively.

factor of two for bound binaries, and greater than two for unbound systems). Such systems are rare, but by definition fall at the widest extreme of the distribution which is what sets the constraints.

The inclusion of unbound binaries in the final distribution contributes the most to weakening the constraints. Fig. 1 shows that at the largest semimajor axis, the total number of binaries is at least one magnitude larger than the number of bound binaries for $M_p > 100\,M_\odot$. The next largest contribution is from the initial semimajor axis distribution. For perturber masses $M_p > 1000\,M_\odot$, the fraction of DM that could consist of compact objects (Fig. 4) increases from 0.1 to 0.3 when comparing a variable distribution ($0 < A < 1$) with a power-law distribution ($A = 1$). Comparing projected separations, and therefore taking into account the large apastron distance of wide binaries, is likely to have had a relatively small effect on the final constraints. While the number of binaries at the largest separations, which are most susceptible to this effect, are the most important for calculating constraints, the increase in binary separation due to this effect is approximately a factor of 2 in most cases.

4 SUMMARY

We have revisited the theoretical modelling involved in placing constraints on the fraction of the MW halo in compact objects from the dynamical effects on the semimajor axis distribution of wide binary stars. We have improved on previous work in several ways. We have used a physically motivated model for the initial binary semimajor axis, taken into account the uncertainty in relating semimajor axis to observed angular separation, and retained unbound binaries. We compare simulated binary separations with observations using the Y^2 statistic (Lucy 2000). This retains the advantages of the χ^2 statistic, namely it allows the goodness of fit of the best fit to be checked and (unlike the K–S test) is sensitive to deviations at the extremes of the distributions.

We find that with these improvements the constraints obtained using the Allen & Monroy-Rodríguez (2014) wide binary sample are significantly weakened. We find $f_{co} < 1$ for $M_{co} \approx 300\,M_\odot$, tightening with increasing M_{co} to $f_{co} < 0.26$ for $M_{co} \gtrsim 1000\,M_\odot$, whereas Monroy-Rodríguez & Allen (2014) found $f_{co} < 1$ for $M_p \sim 10\,M_\odot$, tightening with increasing M_{co} to $f_{co} < 0.1$ for $M_{co} \gtrsim 100\,M_\odot$. It is, therefore, crucial that these modelling improvements are implemented when calculating constraints on compact objects using future improved catalogues of halo wide-binaries.

ACKNOWLEDGEMENTS

ET was supported by a United Kingdom Science and Technology Facilities Council (STFC) studentship. AMG is supported by STFC grant ST/P000703/1.

For the purpose of open access, the authors have applied a CC BY public copyright licence to any author accepted manuscript version arising. This research has made use of the SIMBAD data base, operated at CDS, Strasbourg, France.

DATA AVAILABILITY

This work is entirely theoretical, and has no associated data.

REFERENCES

Abbott B. P. et al., 2016, Phys. Rev. Lett., 116, 061102
Afshordi N., McDonald P., Spergel D. N., 2003, ApJ, 594, L71
Ali-Haïmoud Y., Kamionkowski M., 2017, Phys. Rev. D, 95, 043534
Ali-Haïmoud Y., Kovetz E. D., Kamionkowski M., 2017, Phys. Rev. D, 96, 123523
Allen C., Monroy-Rodríguez M. A., 2014, ApJ, 790, 158
Bahcall J. N., Hut P., Tremaine S., 1985, ApJ, 290, 15
Bertone G., Hooper D., Silk J., 2005, Phys. Rep., 405, 279

Binney J., Tremaine S., 2008, Galactic Dynamics, 2nd edn., Princeton Univ. Press
Bird S., Cholis I., Muñoz J. B., Ali-Haïmoud Y., Kamionkowski M., Kovetz E. D., Raccanelli A., Riess A. G., 2016, Phys. Rev. Lett., 116, 201301
Blaineau T. et al., 2022, A&A, 664, A106
Bovy J., 2015, ApJS, 216, 29
Brandt T. D., 2016, ApJ, 824, L31
Carr B., Kuhnel F., 2020, Ann. Rev. Nucl. Part. Sci., 70, 355
Carr B., Kuhnel F., Sandstad M., 2016, Phys. Rev. D, 94, 083504
Chanamé J., Gould A., 2004, ApJ, 601, 289
Coronado J., Sepúlveda M. P., Gould A., Chanamé J., 2018, MNRAS, 480, 4302
de Salas P. F., Widmark A., 2021, Rep. Prog. Phys., 84, 104901
Diego J. M. et al., 2018, ApJ, 857, 25
Duchêne G., Kraus A., 2013, ARA&A, 51, 269
Eilers A.-C., Hogg D. W., Rix H.-W., Ness M. K., 2019, ApJ, 871, 120
El-Badry K., Rix H.-W., 2019, MNRAS, 482, L139
Esteban-Gutiérrez A., Mediavilla E., Jiménez-Vicente J., Agües-Paszkowsky N., Muñoz J. A., Heydenreich S., 2022, ApJ, 929, L17
Gaggero D., Bertone G., Calore F., Connors R. M. T., Lovell M., Markoff S., Storm E., 2017, Phys. Rev. Lett., 118, 241101
Gaia Collaboration, 2018, A&A, 616, A1
Goodwin S. P., Kroupa P., Goodman A., Burkert A., 2007, in Reipurth B., Jewitt D., Keil K., eds, Protostars and Planets V. p. 133
Green A. M., Kavanagh B. J., 2021, J. Phys. G, 48, 043001
Griffiths D., 2019, PhD thesis, Univ. Sheffield
Hawking S., 1971, MNRAS, 152, 75
Inman D., Ali-Haïmoud Y., 2019, Phys. Rev. D, 100, 083528
Jiang Y.-F., Tremaine S., 2010, MNRAS, 401, 977
Kouwenhoven M. B. N., Goodwin S. P., Parker R. J., Davies M. B., Malmberg D., Kroupa P., 2010, MNRAS, 404, 1835
Lucy L. B., 2000, MNRAS, 318, 92
Moeckel N., Bate M. R., 2010, MNRAS, 404, 721
Moeckel N., Clarke C. J., 2011, MNRAS, 415, 1179
Monroy-Rodríguez M. A., Allen C., 2014, ApJ, 790, 159
Nakamura T., Sasaki M., Tanaka T., Thorne K. S., 1997, ApJ, 487, L139
Navarro J. F., Frenk C. S., White S. D. M., 1997, ApJ, 490, 493
Oelkers R. J., Stassun K. G., Dhital S., 2017, AJ, 153, 259
Oh S., Price-Whelan A. M., Hogg D. W., Morton T. D., Spergel D. N., 2017, AJ, 153, 257
Poulin V., Serpico P. D., Calore F., Clesse S., Kohri K., 2017, Phys. Rev. D, 96, 083524
Quinn D., Wilkinson M., Irwin M., Marshall J., Koch A., Belokurov V., 2009, MNRAS, 396, 11
Raghavan D. et al., 2010, ApJS, 190, 1
Reipurth B., Clarke C. J., Boss A. P., Goodwin S. P., Rodríguez L. F., Stassun K. G., Tokovinin A., Zinnecker H., 2014, in Beuther H., Klessen R. S., Dullemond C. P., Henning T., eds, Protostars and Planets VI. Univ. Arizona Press, Tucson, p. 267
Ricotti M., Ostriker J. P., Mack K. J., 2008, ApJ, 680, 829
Sasaki M., Suyama T., Tanaka T., Yokoyama S., 2016, Phys. Rev. Lett., 117, 061101
Tian H.-J., El-Badry K., Rix H.-W., Gould A., 2020, ApJS, 246, 4
Tokovinin A., Lépine S., 2012, AJ, 144, 102
Tyler E., 2022, PhD thesis, Univ. Nottingham
Ward-Duong K. et al., 2015, MNRAS, 449, 2618
Weinberg M. D., Shapiro S. L., Wasserman I., 1987, ApJ, 312, 367
Wenger M. et al., 2000, A&AS, 143, 9
Yoo J., Chaname J., Gould A., 2004, ApJ, 601, 311
Zel'dovich Y. B., Novikov I. D., 1967, Sov. Astron., 10, 602
Zumalacarregui M., Seljak U., 2018, Phys. Rev. Lett., 121, 141101

This paper has been typeset from a TEX/LATEX file prepared by the author.